

Recent development of high power, widely tunable THz quantum cascade laser sources based on difference-frequency generation

M. Razeghi^{a)}, Q. Y. Lu, N. Bandyopadhyay, S. Slivken

Center for Quantum Devices, Department of Electrical Engineering and Computer Science,
Northwestern University, Evanston, Illinois 60208

ABSTRACT

We present the recent development of high performance compact THz sources based on intracavity nonlinear frequency mixing in mid-infrared quantum cascade lasers. Significant performance improvements of our THz sources with respect to the continuous wave THz power output, monolithic THz tuning, and widely frequency are achieved by systematic optimization of the device's active region, waveguide design, and chip bonding strategy. Room temperature continuous wave THz power of more than 10 μ W at 3.4 THz is demonstrated at room temperature. Monolithic THz tuning of a chip-based THz source from 2.6 to 4.2 THz with power up to 0.1 mW is achieved. Surface emission from the substrate via a diffraction grating with THz power up to 0.5 mW is also obtained. The developing characteristics show the potential for these THz sources as local oscillators for many astronomical and medical applications.

Keywords: terahertz, quantum cascade lasers, difference frequency generation, distributed feedback

1. INTRODUCTION

THz sources based on intracavity difference frequency generation (DFG) in mid-IR QCL have shown considerable progress in the past few years [1-8]. When a QCL active region is designed with strong coupling between the lower lasing levels and injector levels, which results in a large nonlinear susceptibility $\chi^{(2)}$, THz emission can be generated within the cavity [9]. Thus, this type of THz source is free from the temperature limitation suffered by the THz QCLs based on direct optical transition, and ideally its working temperature is only limited by the mid-IR QCL which can work well even above 100 °C [10], and can be tuned over a broad waveguide range with broadband heterogeneous active region design [11]. It not only shares the common features of the mid-IR QCLs which are mass reproducible, room temperature operation, low cost, compact size, and high efficiency, but also carries the potential of delivering THz emission with high power in a wide frequency range.

With the recent systematic optimizations, including dual-core design based on single phonon resonance structure [2] for high efficiency and broad gain operation, use of a composite distributed-feedback (DFB) grating with dual period component [1] for purifying and tuning the mid-IR as well as the THz spectra, and use of the epi-down Čerenkov phase-matching scheme [5] for high THz outcoupling efficiency, THz sources based on DFG in QCLs with high THz power up to 1.9 mW [8], and wide tuning range of 1-4.6 THz have been demonstrated [2].

^{a)} email: razeghi@eecs.northwestern.edu

Here we present the recent development of THz sources based on DFG from QCLs, especially with regard to room temperature continuous wave operation, monolithic THz tuning, and THz surface emission, in the following three sections.

2. CONTINUOUS THZ EMISSION AT ROOM TEMPERATURE

The main limiting obstacle of the previous pulsed THz sources based on DFG in QCLs to CW operation at room temperature is the device's excessive internal heating induced by the high threshold current density, and inefficient heat dissipation through epi-up mounting. More specifically, this is mainly induced by the very high threshold electrical power density $J_{th} \times V_{th}$ of about 120 kW/cm², which is too high for CW operation. Here J_{th} and V_{th} are threshold current density and voltage, respectively. Typical CW QCLs operate at a much lower power density of ~20 kW/cm². For the device with Čerenkov phase-matching scheme, the substrate is semi-insulating, nonconductive. A highly doped InGaAs layer acting as the conductive layer is grown prior to the laser waveguide growth. The geometry of all the previous device is ~20 μm for ridge width and 3 mm for cavity length. To achieve room temperature continuous wave operation, the ridge width needs to be reduced to 6-10 μm for better thermal dissipation. However, the loss increases up quickly as the ridge width decreases. To overcome this issue, a double-channel buried ridge waveguide with double-sided injection is designed to reduce the waveguide loss while maintaining the characteristic of side-current pumping for the Čerenkov phase-matching scheme, as shown in Figure 1(a). On the other hand, since the entire epilayer structure is grown on the semi-insulating InP substrate, both the top contact and bottom contact are fabricated on the same side of the wafer. Therefore, the epi-down mounting of this scheme requires a submount that has been patterned with a corresponding patterns, as shown in Figure 1(b).

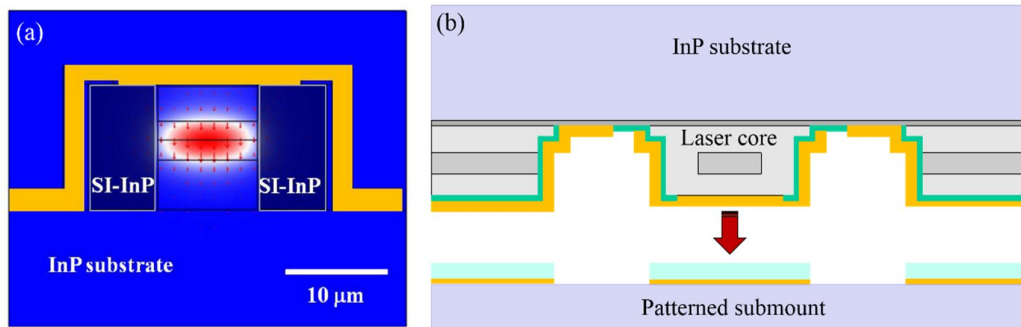


Fig. 1. (a) schematic of double-channel buried ridge waveguide with double-side injection design. (b) schematic of epi-down mounting of a double-channel buried ridge waveguide on a patterned submount.

The wafer is processed into a buried composite DFB and buried ridge waveguide with ridge width of 12 μm and cleaved into 4 mm long cavities. After HR coating on the rear facet, the front facet is polished with an angle of 30°. Then the device is epi-down mounted on a patterned diamond submount. THz power in CW and pulsed mode is tested with a Golay cell detector (Microtech Instruments) assuming 100% collection efficiency. For CW THz power testing, the device is actually modulated with a low frequency pulse (quasi-CW, 40 ms pulse width and 12.5 Hz repetition rate) in order to be compatible with Golay cell detection. Due to the long pulses used, there should be minimal difference in power compared to true CW operation. Figure 2(a) is the THz peak powers in pulsed mode operation tested with different duty cycles from 5% to 30% at 293 K. The power value is not corrected for collection efficiency. A maximum peak power of 28 μW at 5% and a maximum average power of 5.5 μW at 30% are obtained. The mid-IR-to-THz conversion efficiencies are 142 and 190 μW/W², respectively. Following a clear increasing trend

in conversion efficiency with duty cycle, the CW THz power reaches 3 μW with a conversion efficiency of 0.44 mW/W^2 (Fig. 2(b)).

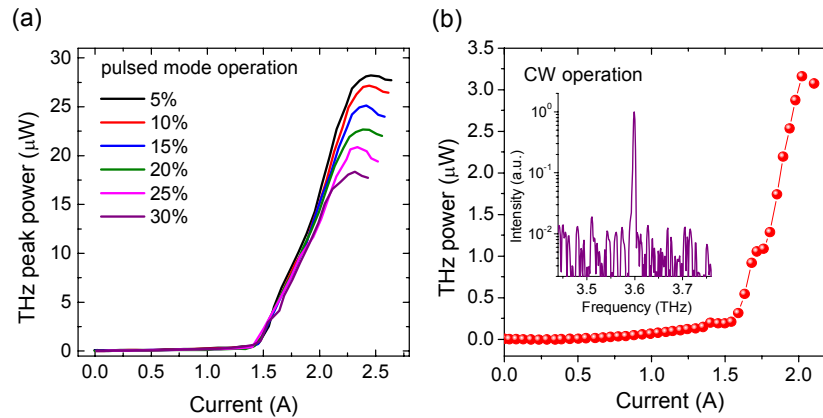


Fig. 2. (a) THz peak power as functions of current at different pulsed duty cycles. (b) THz CW power as a function of current and CW emitting spectrum at 3.6 THz at a current of 1.9 A (inset).

While this power is enough for certain low-power THz applications, higher power can be obtained by either scaling the mid-IR power with longer cavity, or optimizing the nonlinear active region design for higher efficiency. Recently, we demonstrated high power strain-balanced QCL designed with large nonlinear susceptibility for high power CW THz emission based on DFG. A 4-mm long, 12- μm buried-ridge Fabry-Pérot device emits up to 1 W at room temperature continuous wave operation with a wall plug efficiency of 5%. Continuous emission at 3.4 THz with output power more than 10 μW is achieved at room temperature.

3. MONOLITHIC THZ TUNING

A compact, high power, room temperature terahertz source emitting in a wide frequency range ($\sim 1\text{-}5$ THz) will greatly benefit terahertz system development for applications in spectroscopy, communication, sensing, and imaging. The THz source based on DFG in QC has been designed with a broad gain spectrum and a giant nonlinear susceptibility over a broad THz frequency range [2]. Lithographical step tuning from 1.0 to 4.6 THz is first demonstrated from an array of devices [2], and recently enhanced to an even wider tuning from 1.7 to 5.2 THz with an external cavity [4]. Nevertheless, these tunable sources are complex systems, either consisting of several device components lasing at different frequencies or requiring extra movable optical setups.

To overcome these tuning limitations, we recently demonstrated a monolithic tunable THz source based on multi-section sampled-grating distributed feedback-distributed Bragg reflector (SGDFB-DBR) design, as shown in Figure 3(a). The SGDFB QCL technology, developed at Northwestern University, allows for purely electrical tuning of the QCL emission wavelength over a wide range. [12] A QCL wafer with a broadband dual-core active region optimized with large nonlinearities in the 1-5 THz range and CW operation when epi-down mounted is used for this work. A 500-nm InGaAs layer located 100 nm above the laser core is used as the grating host layer. For SGDFB, both sections are sampled with a very short grating section ($\Lambda_0=1.3$ μm , $N_g=13$) for 7 times. The sampling periods $Z_1=270.4$ μm and $Z_2=245.7$ μm are used for the front and back sections, respectively. The estimated Vernier-only

tuning range above is 62.7 cm^{-1} . To enhance the power performance, the SG2 section is further elongated with a 1.5-mm unpatterned section for power amplification.

The measured THz tuning range and characteristics are shown in Figure 3(b). A wide frequency tuning from 2.6 to 4.2 THz with a step of 160-180 GHz is achieved at room temperature by varying the DC currents on the two SG sections, while keeping the DC currents on the DBR section constant. This tuning range corresponds to 47% of the central THz frequency. In the tuned THz frequencies, THz power ranges from $26 \mu\text{W}$ at 2.6 THz to $105 \mu\text{W}$ at 3.64 THz. Since the mid-IR power exhibits only a minor change in power during tuning, the THz power performance as a function of frequency is related mainly to the conversion efficiency characteristic of the device. The conversion efficiency peaks around 3.2-3.8 THz and decreases towards the lower and higher frequency ends. Higher THz power and continuous wave operation can be further obtained by using a device structure with a higher THz conversion efficiency and better thermal packaging [6].

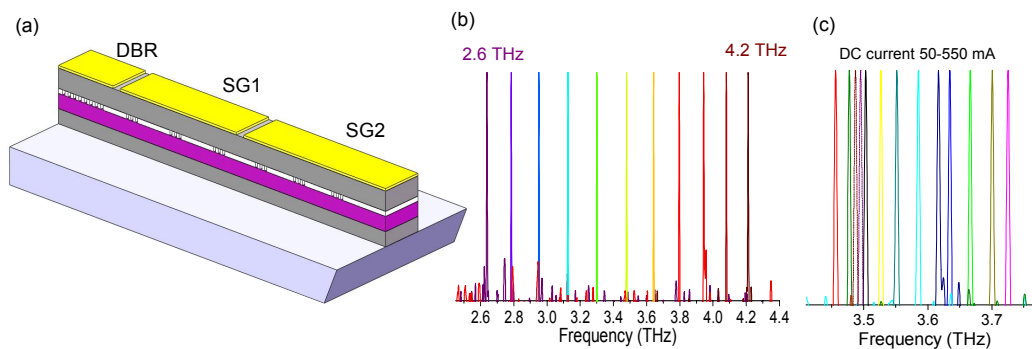


Fig. 3. (a) Schematic of three-section SGDFB-DBR design for THz monolithic tuning. (b) THz Vernier tuning from 2.6-4.2 THz by changing the bias currents on the front two SG sections. (c) THz fine tuning by changing the bias currents on the DBR section. Dashed lines indicate the continuous tuning of THz frequency by changing the DC currents in SG sections simultaneously.

The above Vernier tuning mechanism is not continuous, with a step of 160-180 GHz ($5.3 - 6 \text{ cm}^{-1}$) corresponding to the frequency spacing of the supermodes formed by the sampled gratings. However, the gaps can be bridged by varying the current in the DBR section to tune λ_1 , while the two SG sections are biased with small DC currents (i.e. 40 mA). As shown in Figure 3 (c), a total tuning range of $\sim 10 \text{ cm}^{-1}$ is achieved by changing the DC current from 50-550 mA (corresponding voltage on DBR of $V_{\text{DBR}} \sim 4-9 \text{ V}$). Full continuous tuning of the THz frequency can be achieved by additionally changing the DC currents on the SG sections 1 and 2 simultaneously in step of 40 and 70 mA respectively, as shown in Figure 3(c) (dashed lines). When combined with DBR current tuning, a range of 270 GHz can continuously be covered, as shown in Figure 3(b). This tuning range is much wider than the Vernier tuning step (160-180 GHz), and thus is sufficient to cover the gaps between supermodes.

4. THZ SURFACE EMISSION

All the above Čerenkov THz devices are fabricated on a 350- μm thick semi-insulating InP substrate, and emit the THz light through the polished facet on the substrate with polishing angles of $20-30^\circ$ which is determined by the Čerenkov phase matching angle θ_c of $\theta_c \sim 22^\circ$. This indicates that THz photons in only 860 μm out of the 3-6 mm-long cavity are directly coupled out. The rest of the THz light in the cavity is reflected back into the epilayers and reabsorbed. Further reducing the laser cavity from 3mm to 1mm should be able to enhance the conversion efficiency by 3-7 times but at the price of lower mid-IR and THz powers. In the epi-down mounting scheme, by

integrating a THz diffraction grating or a Si prism to the substrate, THz light in the entire cavity can be outcoupled even for long cavities above 3 mm. Here, we report the first THz surface emission via a first-order diffraction grating patterned on the substrate with a demonstrated THz power up to 0.5 mW.

The QCL structure is based on the single phonon resonance (SPR) dual-core structure with the lattice-matched $\text{In}_{0.53}\text{Ga}_{0.47}\text{As}/\text{In}_{0.52}\text{Al}_{0.48}\text{As}$ laser core grown by gas-source molecular beam epitaxy on a semi-insulating InP substrate. The waveguide structure consists of a 200-nm InGaAs bottom contact layer (Si , $\sim 1 \times 10^{18} \text{ cm}^{-3}$), a 3.5- μm InP buffer (Si , $\sim 1.5 \times 10^{16} \text{ cm}^{-3}$), dual core active region with average doping of $5.3 \times 10^{16} \text{ cm}^{-3}$, a 3.5- μm InP cladding layer (Si , $\sim 1.5 \times 10^{16} \text{ cm}^{-3}$), and a 0.2- μm InP cap layer (Si , $\sim 5 \times 10^{18} \text{ cm}^{-3}$). The wafer is processed into double-channel waveguide with a ridge width of 20 μm . The 1.5-mm long composite DFB section is patterned with a dual-period grating within a 3-mm long laser cavity. The grating is defined on the InP cap layer with a depth of 0.2 μm . The substrate is then polished and is patterned with a first-order diffraction grating by liftoff Ti/Au (10/1500 nm) processing, as shown in Figure 4(a). The grating period Λ_g is defined by $\Lambda_g = \frac{m\lambda_{\text{THz}}}{n_{\text{InP}} \cos \theta_c}$, here λ_{THz} is the THz wavelength, n_{InP} is the InP substrate refractive index in THz wavelength range, and $m=1, 2, 3, \dots$ is the diffraction order. For this work, first-order diffraction grating was designed, with $m=1$.

The THz output power from surface and edge emission in pulsed mode operation with 1% duty cycle was measured using a calibrated Golay cell detector. The THz spectra were taken in rapid scan mode at a resolution of 0.125 cm^{-1} from a Bruker Fourier transform infrared (FTIR) spectrometer equipped with a far-infrared DTGS detector. The initial THz power characterizations of the epi-down bonded devices are shown in Fig. 4(b). The device emits up to 0.5 mW from the surface. Single mode operation at 3.5 THz with side mode suppression ratio up to 30 dB is achieved (inset of Fig. 4(b)). To examine how much power is emitted from the edge, the substrate near the front facet is polished at 25° with respect to the normal cleavage plane. After polishing, the device emits up to 1.0 mW, as shown in Fig. 4(b). The lower surface emission compared to the edge emission is attributed the relatively weak outcoupling efficiency of the metallic diffraction grating. The simulation indicates that only 15% of the generated THz light is outcoupled via the grating. With further optimization to the diffraction efficiency, high THz power up to 3-4 mW is expected.

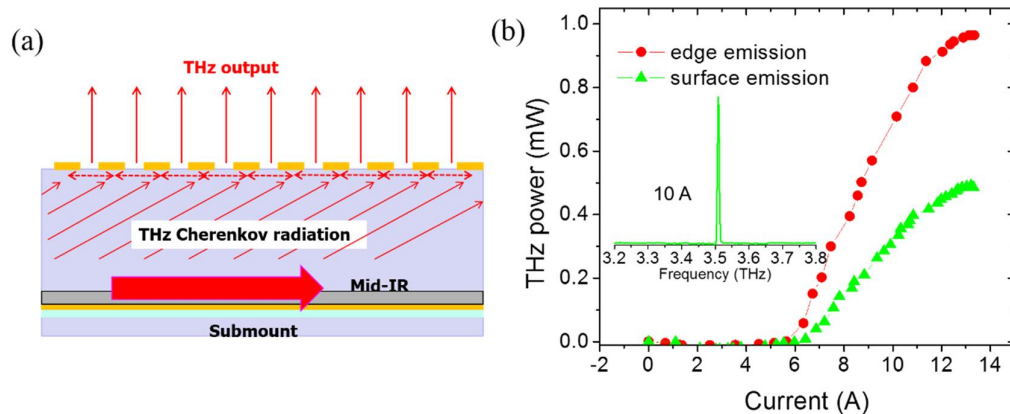


Fig. 4. Mid-IR P-I-V characterizations at different currents for the epil-up and -down mounted devices. Inset: lasing spectra at 10 A for the epi-down mounted device.

In conclusion, we have demonstrated significant performance improvements of room temperature THz sources based on DFG from mid-IR QCLs in the continuous wave operation with THz power more than $10 \mu\text{W}$ at 3.4 THz,

monolithic THz tuning from 2.6 to 4.2 THz with power up to 0.1 mW, and THz surface emission from the substrate via a diffraction grating with THz power up to 0.5 mW. With continued optimization in the waveguide, active region, phase matching scheme, and device package, mW THz power at continuous wave operation in a wide frequency tuning range is achievable from this type of compact device at room temperature.

5. ACKNOWLEDGEMENTS

This work is partially supported by the National Science Foundation (grants ECCS-1231289 and ECCS-1306397, and ECCS-1505409), Department of Homeland Security (grant HSHQDC-13-C-00034), Naval Air Systems Command (grant N68936-13-C-0124), and an Early Stage Innovations grant from NASA's Space Technology Research Grants Program. The authors would also like to acknowledge the encouragement and support of all the involved program managers.

REFERENCES

- [1]. Lu, Q. Y., Bandyopadhyay, N., Slivken, S., Bai, Y., and Razeghi, M., "Room temperature single-mode terahertz sources based on intracavity difference-frequency generation in quantum cascade lasers," *Appl. Phys. Lett.* 99, 131106 (2011).
- [2]. Lu, Q. Y., Bandyopadhyay, N., Slivken, S., Bai, Y., and Razeghi, M., "Widely tuned room temperature terahertz quantum cascade laser sources based on difference-frequency generation," *Appl. Phys. Lett.* 101, 251121 (2012).
- [3]. Lu, Q. Y., Bandyopadhyay, N., Slivken, S., Bai, Y., and Razeghi, M., "High performance terahertz quantum cascade laser sources based on intracavity difference frequency generation," *Optics Express* 21, 968 (2013).
- [4]. Vijayraghavan, K., Jiang, Y., Jang, M., Jiang, A., Choutagunta, K., Vizbaras, A., Demmerle, F., Boehm, G., Amann, M. C., and Belkin, M. A., *Nature Commun.* 4, 2021 (2013).
- [5]. Lu, Q. Y., Bandyopadhyay, N., Slivken, S., Bai, Y., and Razeghi, M., "Room temperature terahertz quantum cascade laser sources with 215 μ W output power through epilayer-down mounting " *Appl. Phys. Lett.* 103, 011101 (2013).
- [6]. Lu, Q. Y., Bandyopadhyay, N., Slivken, S., Bai, Y., and Razeghi, M., "Continuous operation of a monolithic semiconductor terahertz source at room temperature," *Appl. Phys. Lett.* 104, 221105 (2014).
- [7]. Lu, Q. Y., Slivken, S., Bandyopadhyay, N., Bai, Y., and Razeghi, M., "Widely tunable room temperature semiconductor terahertz source," *Appl. Phys. Lett.* 105, 201102 (2014).
- [8]. Razeghi, M., Lu, Q. Y., Bandyopadhyay, N., Zhou, W., Heydari, D., Bai, Y., and Slivken, S., "Quantum cascade lasers: from tool to product", *Optics Express*, 23, 8462 (2015).
- [9]. Belkin, M. A., Capasso, F., Xie, F., Belyanin, A., Fischer, M., Wittmann, A., and Faist, J., "Room temperature terahertz quantum cascade laser source based on intracavity difference-frequency generation," *Appl. Phys. Lett.*, 92, 201101 (2008).
- [10]. Bai, Y., Bandyopadhyay, N., Tsao, S., Slivken, S., and Razeghi, M., "Room temperature quantum cascade lasers with 27% wall plug efficiency," *Appl. Phys. Lett.*, 98, 181102 (2011).

- [11]. Bandyopadhyay, N., Bai, Y., Slivken, S., and Razeghi, M., "High power operation of $\lambda \sim 5.2\text{--}11\ \mu\text{m}$ strain balanced quantum cascade lasers based on the same material composition," *Appl. Phys. Lett.* 105, 071106 (2014).
- [12]. Slivken, S., Bandyopadhyay, N., Bai, Y., Lu, Q. Y., and Razeghi, M., "Extended electrical tuning of quantum cascade lasers with digital concatenated gratings," *Appl. Phys. Lett.* 103, 231110 (2013).